Observation of $e^+e^- \to \eta' J/\psi$ at center-of-mass energies between 4.19 and 4.60 GeV

M. Ablikim[1], M. N. Achasov[9,f], X. C. Ai[1], O. Albayrak[5], M. Albrecht[4], D. J. Ambrose[44], A. Amoroso[49A,49C], F. F. An[1], Q. An[46,a], J. Z. Bai[1], R. Baldini Ferroli[20A], Y. Ban[31], D. W. Bennett[19], J. V. Bennett[5], M. Bertani[20A], D. Bettoni[21A], J. M. Bian[43], F. Bianchi[49A,49C], E. Boger[23,d], I. Boyko[23], R. A. Briere[5], H. Cai[51], X. Cai[1,a], O. Cakir[40A,b], A. Calcaterra[20A], G. F. Cao[1], S. A. Cetin[40B], J. F. Chang[1,a], G. Chelkov[23,d,e], G. Chen[1], H. S. Chen[1], H. Y. Chen[2], J. C. Chen[1], M. L. Chen[1,a], S. J. Chen[29], X. Chen[1,a], X. R. Chen[26], Y. B. Chen[1,a], H. P. Cheng[17], X. K. Chu[31], G. Cibinetto[21A], H. L. Dai[1,a], J. P. Dai[34], A. Dbeyssi[14], D. Dedovich[23], Z. Y. Deng[1], A. Denig[22], I. Denysenko[23], M. Destefanis[49A,49C], F. De Mori[49A,49C], Y. Ding[27], C. Dong[30], J. Dong[1,a], L. Y. Dong[1], M. Y. Dong[1,a], S. X. Du[53], P. F. Duan[1], E. E. Eren[40B], J. Z. Fan[39], J. Fang[1,a], S. S. Fang[1], X. Fang[46,a], Y. Fang[1], L. Fava[49B,49C], F. Feldbauer[22], G. Felici[20A], C. Q. Feng[46,a], E. Fioravanti[21A], M. Fritsch[14,22], C. D. Fu[1], Q. Gao[1], X. Y. Gao[2], Y. Gao[39], Z. Gao[46,a], I. Garzia[21A], K. Goetzen[10], W. X. Gong[1,a], W. Gradl[22], M. Greco[49A,49C], M. H. Gu[1,a], Y. T. Gu[12], Y. H. Guan[1], A. Q. Guo[1], L. B. Guo[28], Y. Guo[1], Y. P. Guo[22], Z. Haddadi[25], A. Hafner[22], S. Han[51], X. Q. Hao[15], F. A. Harris[42], K. L. He[1], X. Q. He[45], T. Held[4], Y. K. Heng[1,a], Z. L. Hou[1], C. Hu[28], H. M. Hu[1], J. F. Hu[49A,49C], T. Hu[1,a], Y. Hu[1], G. M. Huang[6], G. S. Huang[46,a], J. S. Huang[15], X. T. Huang[33], Y. Huang[29], T. Hussain[48], Q. Ji[1], Q. P. Ji[30], X. B. Ji[1], X. L. Ji[1,a], L. W. Jiang[51], X. S. Jiang[1,a], X. Y. Jiang[30], J. B. Jiao[33], Z. Jiao[17], D. P. Jin[1,a], S. Jin[1], T. Johansson[50], A. Julin[43], N. Kalantar-Nayestanaki[25], X. L. Kang[1], X. S. Kang[30], M. Kavatsyuk[25], B. C. Ke[5], P. Kiese[22], R. Kliemt[14], B. Kloss[22], O. B. Kolcu[40B,i], B. Kopf[4], M. Kornicer[42], W. Kuehn[24], A. Kupsc[50], J. S. Lange[24], M. Lara[19], P. Larin[14], C. Leng[49C], C. Li[50], Cheng Li[46,a], D. M. Li[53], F. Li[1,a], F. Y. Li[31], G. Li[1], H. B. Li[1], J. C. Li[1], Jin Li[32], K. Li[33], K. Li[13], Lei Li[3], P. R. Li[41], T. Li[33], W. D. Li[1], W. G. Li[1], X. L. Li[33], X. M. Li[12], X. N. Li[1,a], X. Q. Li[30], Z. B. Li[38], H. Liang[46,a], Y. F. Liang[36], Y. T. Liang[24], G. R. Liao[11], D. X. Lin[14], B. J. Liu[1], C. X. Liu[1], F. H. Liu[35], Fang Liu[1], Feng Liu[6], H. B. Liu[12], H. H. Liu[16], H. H. Liu[1], H. M. Liu[1], J. Liu[1], J. B. Liu[46,a], J. P. Liu[51], J. Y. Liu[1], K. Liu[39], K. Y. Liu[27], L. D. Liu[31], P. L. Liu[1,a], Q. Liu[41], S. B. Liu[46,a], X. Liu[26], Y. B. Liu[30], Z. A. Liu[1,a], Zhiqing Liu[22], H. Loehner[25], X. C. Lou[1,a,h], H. J. Lu[17], J. G. Lu[1,a], Y. Lu[1], Y. P. Lu[1,a], C. L. Luo[28], M. X. Luo[52], T. Luo[42], X. L. Luo[1,a], X. R. Lyu[41], F. C. Ma[27], H. L. Ma[1], L. L. Ma[33], Q. M. Ma[1], T. Ma[1], X. N. Ma[30], X. Y. Ma[1,a], F. E. Maas[14], M. Maggiora[49A,49C], Y. J. Mao[31], Z. P. Mao[1], S. Marcello[49A,49C], J. G. Messchendorp[25], J. Min[1,a], R. E. Mitchell[19], X. H. Mo[1,a], Y. J. Mo[6], C. Morales Morales[14], K. Moriya[19], N. Yu. Muchnoi[9,f], H. Muramatsu[43], Y. Nefedov[23], F. Nerling[14], I. B. Nikolaev[9,f], Z. Ning[1,a], S. Nisar[8], S. L. Niu[1,a], X. Y. Niu[1], S. L. Olsen[32], Q. Ouyang[1,a], S. Pacetti[20B], P. Patteri[20A], M. Pelizaeus[4], H. P. Peng[46,a], K. Peters[10], J. Pettersson[50], J. L. Ping[28], R. G. Ping[1], R. Poling[43], V. Prasad[1], M. Qi[29], S. Qian[1,a], C. F. Qiao[41], L. Q. Qin[33], N. Qin[51], X. S. Qin[1], Z. H. Qin[1,a], J. F. Qiu[1], K. H. Rashid[48], C. F. Redmer[22], M. Ripka[22], G. Rong[1], Ch. Rosner[14], X. D. Ruan[12], V. Santoro[21A], A. Sarantsev[23,g], M. Savrié[21B], K. Schoenning[50], S. Schumann[22], W. Shan[31], M. Shao[46,a], C. P. Shen[2], P. X. Shen[30], X. Y. Shen[1], H. Y. Sheng[1], W. M. Song[1], X. Y. Song[1], S. Sosio[49A,49C], S. Spataro[49A,49C],

G. X. Sun[1], J. F. Sun[15], S. S. Sun[1], Y. J. Sun[46,a], Y. Z. Sun[1], Z. J. Sun[1,a], Z. T. Sun[19], C. J. Tang[36], X. Tang[1], I. Tapan[40C], E. H. Thorndike[44], M. Tiemens[25], M. Ullrich[24], I. Uman[40B], G. S. Varner[42], B. Wang[30], D. Wang[31], D. Y. Wang[31], K. Wang[1,a], L. L. Wang[1], L. S. Wang[1], M. Wang[33], P. Wang[1], P. L. Wang[1], S. G. Wang[31], W. Wang[1,a], X. F. Wang[39], Y. D. Wang[14], Y. F. Wang[1,a], Y. Q. Wang[22], Z. Wang[1,a], Z. G. Wang[1,a], Z. H. Wang[46,a], Z. Y. Wang[1], T. Weber[22], D. H. Wei[11], J. B. Wei[31], P. Weidenkaff[22], S. P. Wen[1], U. Wiedner[4], M. Wolke[50], L. H. Wu[1], Z. Wu[1,a], L. G. Xia[39], Y. Xia[18], D. Xiao[1], H. Xiao[47], Z. J. Xiao[28], Y. G. Xie[1,a], Q. L. Xiu[1,a], G. F. Xu[1], L. Xu[1], Q. J. Xu[13], X. P. Xu[37], L. Yan[46,a], W. B. Yan[46,a], W. C. Yan[46,a], Y. H. Yan[18], H. J. Yang[34], H. X. Yang[1], L. Yang[51], Y. Yang[6], Y. X. Yang[11], M. Ye[1,a], M. H. Ye[7], J. H. Yin[1], B. X. Yu[1,a], C. X. Yu[30], J. S. Yu[26], C. Z. Yuan[1], W. L. Yuan[29], Y. Yuan[1], A. Yuncu[40B,c], A. A. Zafar[48], A. Zallo[20A], Y. Zeng[18], B. X. Zhang[1], B. Y. Zhang[1,a], C. Zhang[29], C. C. Zhang[1], D. H. Zhang[1], H. H. Zhang[38], H. Y. Zhang[1,a], J. J. Zhang[1], J. L. Zhang[1], J. Q. Zhang[1], J. W. Zhang[1,a], J. Y. Zhang[1], J. Z. Zhang[1], K. Zhang[1], L. Zhang[1], X. Y. Zhang[33], Y. Zhang[1], Y. N. Zhang[41], Y. H. Zhang[1,a], Y. T. Zhang[46,a], Yu Zhang[41], Z. H. Zhang[6], Z. P. Zhang[46], Z. Y. Zhang[51], G. Zhao[1], J. W. Zhao[1,a], J. Y. Zhao[1], J. Z. Zhao[1,a], Lei Zhao[46,a], Ling Zhao[1], M. G. Zhao[30], Q. Zhao[1], Q. W. Zhao[1], S. J. Zhao[53], T. C. Zhao[1], Y. B. Zhao[1,a], Z. G. Zhao[46,a], A. Zhemchugov[23,d], B. Zheng[47], J. P. Zheng[1,a], W. J. Zheng[33], Y. H. Zheng[41], B. Zhong[28], L. Zhou[1,a], X. Zhou[51], X. K. Zhou[46,a], X. R. Zhou[46,a], X. Y. Zhou[1], K. Zhu[1], K. J. Zhu[1,a], S. Zhu[1], S. H. Zhu[45], X. L. Zhu[39], Y. C. Zhu[46,a], Y. S. Zhu[1], Z. A. Zhu[1], J. Zhuang[1,a], L. Zotti[49A,49C], B. S. Zou[1], J. H. Zou[1]

(BESIII Collaboration)

[1] *Institute of High Energy Physics, Beijing 100049, People's Republic of China*
[2] *Beihang University, Beijing 100191, People's Republic of China*
[3] *Beijing Institute of Petrochemical Technology, Beijing 102617, People's Republic of China*
[4] *Bochum Ruhr-University, D-44780 Bochum, Germany*
[5] *Carnegie Mellon University, Pittsburgh, Pennsylvania 15213, USA*
[6] *Central China Normal University, Wuhan 430079, People's Republic of China*
[7] *China Center of Advanced Science and Technology, Beijing 100190, People's Republic of China*
[8] *COMSATS Institute of Information Technology, Lahore, Defence Road, Off Raiwind Road, 54000 Lahore, Pakistan*
[9] *G.I. Budker Institute of Nuclear Physics SB RAS (BINP), Novosibirsk 630090, Russia*
[10] *GSI Helmholtzcentre for Heavy Ion Research GmbH, D-64291 Darmstadt, Germany*
[11] *Guangxi Normal University, Guilin 541004, People's Republic of China*
[12] *GuangXi University, Nanning 530004, People's Republic of China*
[13] *Hangzhou Normal University, Hangzhou 310036, People's Republic of China*
[14] *Helmholtz Institute Mainz, Johann-Joachim-Becher-Weg 45, D-55099 Mainz, Germany*
[15] *Henan Normal University, Xinxiang 453007, People's Republic of China*
[16] *Henan University of Science and Technology, Luoyang 471003, People's Republic of China*
[17] *Huangshan College, Huangshan 245000, People's Republic of China*
[18] *Hunan University, Changsha 410082, People's Republic of China*
[19] *Indiana University, Bloomington, Indiana 47405, USA*

[20] *(A)INFN Laboratori Nazionali di Frascati, I-00044, Frascati, Italy; (B)INFN and University of Perugia, I-06100, Perugia, Italy*
[21] *(A)INFN Sezione di Ferrara, I-44122, Ferrara, Italy; (B)University of Ferrara, I-44122, Ferrara, Italy*
[22] *Johannes Gutenberg University of Mainz, Johann-Joachim-Becher-Weg 45, D-55099 Mainz, Germany*
[23] *Joint Institute for Nuclear Research, 141980 Dubna, Moscow region, Russia*
[24] *Justus Liebig University Giessen, II. Physikalisches Institut, Heinrich-Buff-Ring 16, D-35392 Giessen, Germany*
[25] *KVI-CART, University of Groningen, NL-9747 AA Groningen, The Netherlands*
[26] *Lanzhou University, Lanzhou 730000, People's Republic of China*
[27] *Liaoning University, Shenyang 110036, People's Republic of China*
[28] *Nanjing Normal University, Nanjing 210023, People's Republic of China*
[29] *Nanjing University, Nanjing 210093, People's Republic of China*
[30] *Nankai University, Tianjin 300071, People's Republic of China*
[31] *Peking University, Beijing 100871, People's Republic of China*
[32] *Seoul National University, Seoul, 151-747 Korea*
[33] *Shandong University, Jinan 250100, People's Republic of China*
[34] *Shanghai Jiao Tong University, Shanghai 200240, People's Republic of China*
[35] *Shanxi University, Taiyuan 030006, People's Republic of China*
[36] *Sichuan University, Chengdu 610064, People's Republic of China*
[37] *Soochow University, Suzhou 215006, People's Republic of China*
[38] *Sun Yat-Sen University, Guangzhou 510275, People's Republic of China*
[39] *Tsinghua University, Beijing 100084, People's Republic of China*
[40] *(A)Istanbul Aydin University, 34295 Sefakoy, Istanbul, Turkey; (B)Dogus University, 34722 Istanbul, Turkey; (C)Uludag University, 16059 Bursa, Turkey*
[41] *University of Chinese Academy of Sciences, Beijing 100049, People's Republic of China*
[42] *University of Hawaii, Honolulu, Hawaii 96822, USA*
[43] *University of Minnesota, Minneapolis, Minnesota 55455, USA*
[44] *University of Rochester, Rochester, New York 14627, USA*
[45] *University of Science and Technology Liaoning, Anshan 114051, People's Republic of China*
[46] *University of Science and Technology of China, Hefei 230026, People's Republic of China*
[47] *University of South China, Hengyang 421001, People's Republic of China*
[48] *University of the Punjab, Lahore-54590, Pakistan*
[49] *(A)University of Turin, I-10125, Turin, Italy; (B)University of Eastern Piedmont, I-15121, Alessandria, Italy; (C)INFN, I-10125, Turin, Italy*
[50] *Uppsala University, Box 516, SE-75120 Uppsala, Sweden*
[51] *Wuhan University, Wuhan 430072, People's Republic of China*
[52] *Zhejiang University, Hangzhou 310027, People's Republic of China*
[53] *Zhengzhou University, Zhengzhou 450001, People's Republic of China*

[a] *Also at State Key Laboratory of Particle Detection and Electronics, Beijing 100049, Hefei 230026, People's Republic of China*
[b] *Also at Ankara University,06100 Tandogan, Ankara, Turkey*

[c] Also at Bogazici University, 34342 Istanbul, Turkey
[d] Also at the Moscow Institute of Physics and Technology, Moscow 141700, Russia
[e] Also at the Functional Electronics Laboratory, Tomsk State University, Tomsk, 634050, Russia
[f] Also at the Novosibirsk State University, Novosibirsk, 630090, Russia
[g] Also at the NRC "Kurchatov Institute, PNPI, 188300, Gatchina, Russia
[h] Also at University of Texas at Dallas, Richardson, Texas 75083, USA
[i] Also at Istanbul Arel University, 34295 Istanbul, Turkey

(Dated: November 11, 2015)

The process $e^+e^- \to \eta' J/\psi$ is observed for the first time with a statistical significance of 8.6σ at $\sqrt{s} = 4.230$ GeV and 7.3σ at $\sqrt{s} = 4.260$ GeV using data samples collected with the BESIII detector. The Born cross sections are measured to be $(3.7 \pm 0.7 \pm 0.3)$ and $(3.9 \pm 0.8 \pm 0.3)$ pb at $\sqrt{s} = 4.230$ and 4.260 GeV, respectively, where the first errors are statistical and the second ones systematic. Upper limits at 90% confidence level of the Born cross sections are also reported at other 12 center-of-mass energies, because of the absence of $\eta' J/\psi$ signal.

I. INTRODUCTION

The region at center-of-mass (c.m.) energies above the open charm threshold is of great interest to theory due to its richness of charmonium states, whose properties are not well understood. Until now, the $\psi(3770)$, $\psi(4040)$, $\psi(4160)$, and $\psi(4415)$, are well established experimentally in the hadronic cross section in e^+e^- annihilation [1], match very well with the calculation in the quark model of charmonium [1]. Exploiting initial state radiation (ISR), the B-factories BaBar and Belle have discovered several new vector charmonium-like states, the $Y(4260)$, $Y(4360)$, and $Y(4660)$, via their decays into the hidden-charm $\pi^+\pi^- J/\psi$ or $\pi^+\pi^-\psi(3686)$ final states [2–6]. While there is no corresponding Y-structures observed in open-charm production and in inclusive hadronic final states, there is no evident excited ψ states in the above two hidden-charm final states. The overpopulation of the vector states between 4.0 and 4.7 GeV triggered many discussions on the nature of these states and possible discovery of new kinds of hadrons [7].

Besides the $\pi^+\pi^-$ hadronic transitions, information on other hadronic transitions will provide further insight for the internal structure of these charmonium and charmonium-like states. CLEO-c, BESIII, and Belle measured the cross section of $e^+e^- \to \eta J/\psi$ [8–10], which has significant contribution from the $\psi(4040)$ and $\psi(4160)$ decays which is different from the prediction in Ref. [11] by considering the virtual charmed meson loops. Treating η and η' with the Light-Cone approach and J/ψ with non-relativistic QCD, and adding the contribution of the resonance decays, authors of Ref. [12] can reproduce the measured $e^+e^- \to \eta J/\psi$ line shape, and the production cross section of the analogous process $e^+e^- \to \eta' J/\psi$ is predicted for c.m. energy $\sqrt{s}$ from 4.3 to 5.3 GeV.

To check the model predictions [12] and to search for potential $\eta' J/\psi$ transition from charmonium and charmonium-like states, we measure $e^+e^- \to \eta' J/\psi$ with all the available data at BESIII. The investigation of this process with data at $\sqrt{s}$ from 3.970 to 4.260 GeV has been performed at CLEO-c experiment, no signal was observed [8].

In this paper, we report the Born cross section measurements for $e^+e^- \to \eta' J/\psi$ at 14 energy points for $\sqrt{s}$ from 4.19 to 4.60 GeV [13]. The data samples are collected with the BESIII [14] detector operating at BEPCII storage ring. The total integrated luminosity is about 4.5 fb^{-1}, which is measured using large angle Bhabha events with an uncertainty of 1% [15]. In the analysis, the J/ψ is reconstructed through its decays into lepton pairs $J/\psi \to \ell^+\ell^-$ ($\ell = e$ or μ) while η' is reconstructed with two decay channels, $\eta' \to \eta\pi^+\pi^-$ (with $\eta \to \gamma\gamma$) and $\eta' \to \gamma\pi^+\pi^-$.

II. DETECTOR AND MONTE CARLO SIMULATION

BESIII [14] is an upgrade of the BESII experiment at the BEPC accelerator [16] for studies of hadron spectroscopy and physics in the τ-charm energy region [17]. The design peak luminosity of the double-ring e^+e^- collider, BEPCII, is 10^{33} cm^{-2}s^{-1} at a beam current of 0.93 A and $\sqrt{s} = 3.77$ GeV.

The BESIII detector with a geometrical acceptance of 93% of 4π, consists of the following main components: 1) a main drift chamber (MDC) equipped with 6796 signal wires and 21884 field wires arranged in a small cell configuration with 43 layers working in a gas mixture of He(40%) and C_3H_8(60%). The single wire resolution on average is 135 μm and the momentum resolution for charged particles in a 1 T magnetic field is 0.5% at 1 GeV; 2) an electromagnetic calorimeter (EMC) made of 6240 CsI(Tl) crystals arranged in a cylindrical shape, complemented by two endcaps. The energy resolution is 2.5% in the barrel and 5% in the endcaps at 1.0 GeV; the position resolution is 6 mm in the barrel and 9 mm in the endcaps at 1.0 GeV. The time resolution of the EMC is 50 ns. 3) a time-of-flight system (TOF) for particle identification made of 176 pieces of 5 cm thick, 2.4 m long plastic scintillators arranged as a cylinder with two layers for the barrel, and 96 fan-shaped, 5 cm thick, plastic scintillators for two end-caps. The time resolution is 80 ps in the barrel, and 110 ps in the end-caps, corresponding to a K/π separation at 2σ level up to about 1.0 GeV; 4) a muon chamber system (MUC) made of resistive plate chambers (RPC) arranged in 9 layers in the barrel and 8 layers in the endcaps, with a resolution of 2 cm.

In order to optimize the selection criteria, determine the detection efficiency and estimate the potential background, the Monte Carlo (MC) samples are generated based on GEANT4 [18] software. The signal MC samples of $e^+e^- \to \eta' J\psi$ are generated at each c.m. energy point assuming the Born cross section follows an incoherent sum of a Breit-Wigner (BW) function for the $\psi(4160)$ resonance and a polynomial term for the continuum production. For the background study, inclusive MC samples including the $Y(4260)$ decays, ISR production of the vector charmonium states, continuum production of hadrons and QED processes are generated with KKMC [19, 20] at $\sqrt{s} = 4.260$, 4.420, and 4.600 GeV. For the inclusive MC samples, the main known decay modes are generated with EVTGEN [20], and the remaining events associated with charmonium decays are generated with LUNDCHARM [21] model, while continuum hadronic events are generated with PYTHIA [22].

III. EVENT SELECTION AND STUDY OF BACKGROUND SHAPE

The candidate events of $e^+e^- \to \eta' J/\psi$ are required to have four charged tracks with zero net charge. All charged tracks are required to be well reconstructed in the MDC with good helix fit quality and to satisfy $|\cos\theta| < 0.93$, where θ is the polar angle of the track in the laboratory frame. The charged tracks are required to originate from the interaction region, with $R_{xy} < 1.0$ cm and $|R_z| < 10.0$ cm, where R_{xy} and R_z are the closest approach of the charged track perpendicular to and along the beam direction, respectively. A charged track with momentum less than 0.8 GeV is assigned to be a pion candidate while a track with momentum larger than 1.0 GeV is assigned to be a lepton candidate. Electron and muon separation is carried out by the ratio (E/p) of energy deposited in EMC and momentum measured in MDC. For electron candidates, we required an E/p ratio larger than 0.8; while for muon candidates, the E/p ratio is required to be less than 0.4.

Photon candidates are reconstructed with showers in EMC crystals. The minimum energy of photon is required to be 25 MeV in the barrel ($|\cos\theta| < 0.80$) and 50 MeV in the end-cap ($0.86 < |\cos\theta| < 0.92$). To eliminate showers produced by charged particles, the angle between the shower and nearest charged track is required to be greater than 20 degrees. EMC cluster timing is further required to be larger than 0 and less than 14 ($\times$ 50 ns) to suppress electronic noise and energy deposits unrelated to the event. The number of good photons is required to be at least 1 for $\eta' \to \gamma\pi^+\pi^-$ and at least 2 for $\eta' \to \eta\pi^+\pi^-$.

For $\eta' \to \gamma\pi^+\pi^-$, a four-constraint (4C) kinematic fit is performed on four selected charged tracks ($\pi^+\pi^-e^+e^-$ or $\pi^+\pi^-\mu^+\mu^-$) and one good photon candidate to improve the momentum and energy resolutions of the final-state particles and to reduce potential background. If there is more than one photon in an event, the one with minimum $\chi^2_{\rm 4C}$ of the kinematic fit is retained for further study. The $\chi^2_{\rm 4C}$ is required to be less than 40. For $\eta' \to \eta\pi^+\pi^-$, a five-constraint (5C) kinematic fit is performed on four charged tracks ($\pi^+\pi^-e^+e^-$ or $\pi^+\pi^-\mu^+\mu^-$) and two good photon candidates, with the constraint of the invariant mass of $\gamma\gamma$ to be equal to the nominal mass of η [1]. For events with more than two photons, the combination with the minimum $\chi^2_{\rm 5C}$ is chosen. The $\chi^2_{\rm 5C}$ is required to be less than 40.

Besides the requirements described above, the following selection criteria are further implemented to select the signal. In $\eta' \to \gamma\pi^+\pi^-$, to eliminate the backgrounds from ISR processes with $\psi(3686)$ in final state or from process $e^+e^- \to \pi^+\pi^- J/\psi$ with final state radiation (FSR) from leptons, the invariant mass of $\pi^+\pi^- J/\psi$ ($M(\pi^+\pi^- J/\psi)$) and the recoiling mass of $\pi^+\pi^-$ ($M^{\rm recoil}(\pi^+\pi^-)$) are required to be out of the regions $3.65 < M(\pi^+\pi^- J/\psi) < 3.71$ GeV and $3.05 < M^{\rm recoil}(\pi^+\pi^-) < 3.15$ GeV, respectively. In $\eta' \to \eta\pi^+\pi^-$, the corresponding distributions are required to be out of the regions $3.67 < M(\pi^+\pi^- J/\psi) < 3.71$ GeV and $3.65 < M^{\rm recoil}(\pi^+\pi^-) < 3.69$ GeV to eliminate the backgrounds $e^+e^- \to \eta\psi(3686) \to \eta\pi^+\pi^- J/\psi$ and $e^+e^- \to \pi^+\pi^-\psi(3686) \to \pi^+\pi^-\eta J/\psi$, respectively.

After applying the above selection criteria, Fig. 1 shows the invariant mass distribution of $\ell^+\ell^-$ for events with the invariant mass of $\gamma(\eta)\pi^+\pi^-$ within the η' signal and sideband regions for the data samples at $\sqrt{s} = 4.230$ and 4.260 GeV. Here the η' signal region is defined as $(0.94, 0.98)$ GeV, while η' sideband regions are $(0.90, 0.94)$ GeV and $(0.98, 1.02)$ GeV. The J/ψ signals are observed clearly at both energy points. A small peaking background evident around the J/ψ peak comes from $e^+e^- \to \gamma_{\rm ISR}\pi^+\pi^- J/\psi$ according to the MC study, which

does not produce peaking background in the distribution of $M(\gamma\pi^+\pi^-)$. The mass window requirement $3.07 < M(\ell^+\ell^-) < 3.13$ GeV is used to select J/ψ signal for further study. After imposing all these selection criteria, the background contribution is investigated with the inclusive MC samples. The dominant backgrounds are found to be those with the same final states as the signal events but without η' or J/ψ intermediate states, and can not be removed completely.

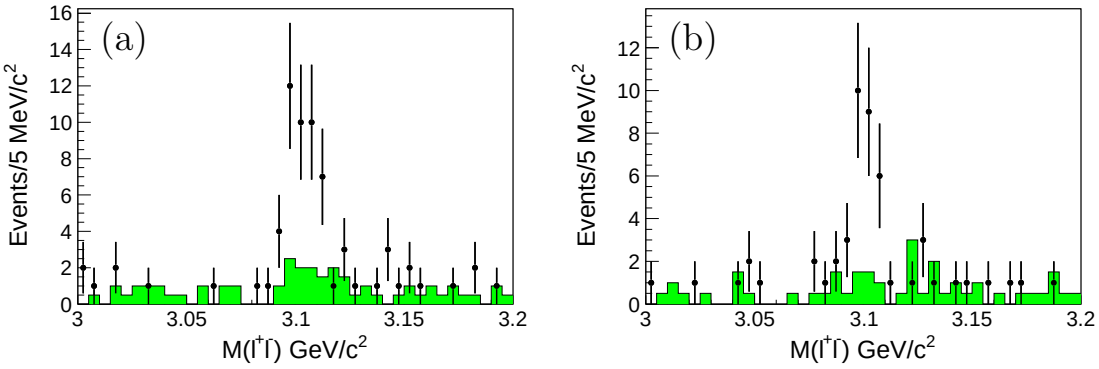

FIG. 1: The $M(\ell^+\ell^-)$ distribution of data summed over the four channels ($\eta' \to \eta\pi^+\pi^-/\gamma\pi^+\pi^-$ and $J/\psi \to e^+e^-/\mu^+\mu^-$) at $\sqrt{s} = 4.230\,\text{GeV}$ (a) and $\sqrt{s} = 4.260\,\text{GeV}$ (b). The dots with error bars and the (green) shaded histograms represent events within η' signal and sideband regions, respectively.

IV. SIGNAL EXTRACTION

After implementing all of above selection criteria except for the η' mass window requirement, the invariant mass distributions of $\gamma\pi^+\pi^-$ and $\eta\pi^+\pi^-$ for $J/\psi \to e^+e^-$ and $J/\psi \to \mu^+\mu^-$ are shown in Fig. 2 for the data at $\sqrt{s}$=4.230 GeV, and Fig. 3 for the data at $\sqrt{s}$=4.260 GeV. When the four channels are combined, η' signal is observed clearly. The background is assumed to be flat in $\gamma\pi^+\pi^-$ final states by studying the corresponding distributions of the events in the J/ψ sideband region and of the MC samples, while the distribution of invariant mass of $\eta\pi^+\pi^-$ is essentially background-free.

To extract the signal yields, a simultaneous fit on the invariant mass of $\gamma(\eta)\pi^+\pi^-$ with an unbinned maximum likelihood method is performed for the four different channels. In the fit, the total signal yields, denoted as $N_{\rm tot}$, is floated. The signal yields for the individual decay mode is constrained by assuming the same production cross section for $e^+e^- \to \eta' J/\psi$ and is determined to be $N_{\rm tot} \times \mathcal{B}(\eta') \times \mathcal{B}(J/\psi) \times \epsilon$, where, $\mathcal{B}(\eta')$ and $\mathcal{B}(J/\psi)$ are the decay branching fractions of η' and J/ψ, respectively, and ϵ is the corresponding detection efficiency. The η' signal is described by a MC simulated shape convolved with a Gaussian function to take into account the mass resolution difference between data and the MC simulation, the parameters of Gaussian function are free but constrained to be the same for different channels. The background is described with a linear function, and its normalization factors are allowed to float in different channels.

The mode-by-mode and combined fit results at $\sqrt{s} = 4.230\,\text{GeV}$ are shown in Fig. 2. The

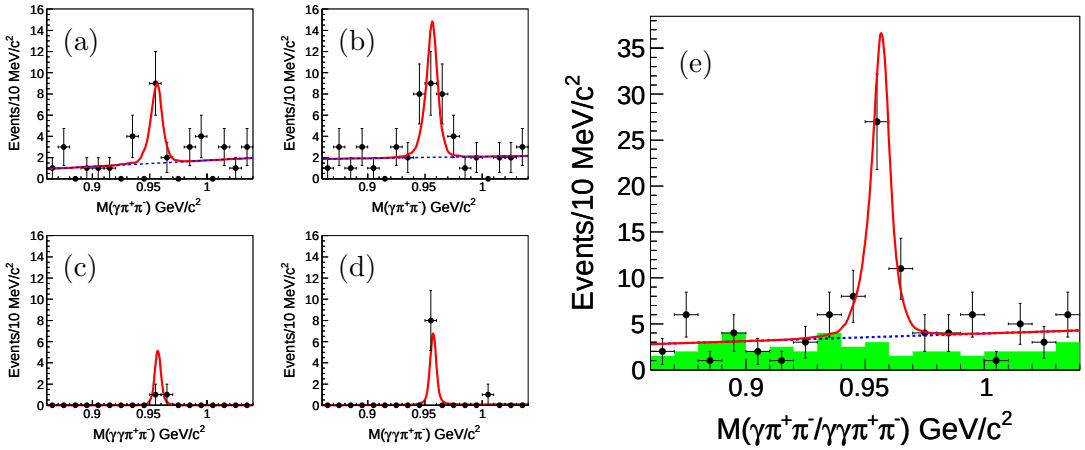

FIG. 2: Simultaneous fit to the $M(\gamma\pi^+\pi^-/\gamma\gamma\pi^+\pi^-)$ spectra at $\sqrt{s} = 4.230\,\text{GeV}$. (a) for $\eta' \to \gamma\pi^+\pi^-$ and $J/\psi \to e^+e^-$, (b) for $\eta' \to \gamma\pi^+\pi^-$ and $J/\psi \to \mu^+\mu^-$, (c) for $\eta' \to \eta\pi^+\pi^-$ and $J/\psi \to e^+e^-$, (d) for $\eta' \to \eta\pi^+\pi^-$ and $J/\psi \to \mu^+\mu^-$. (e) shows the combined result. The dots with error bars and the (green) shaded histograms represent events from data within J/ψ signal region and sideband region, respectively. The solid lines show the fit results, while the dashed lines represent the background.

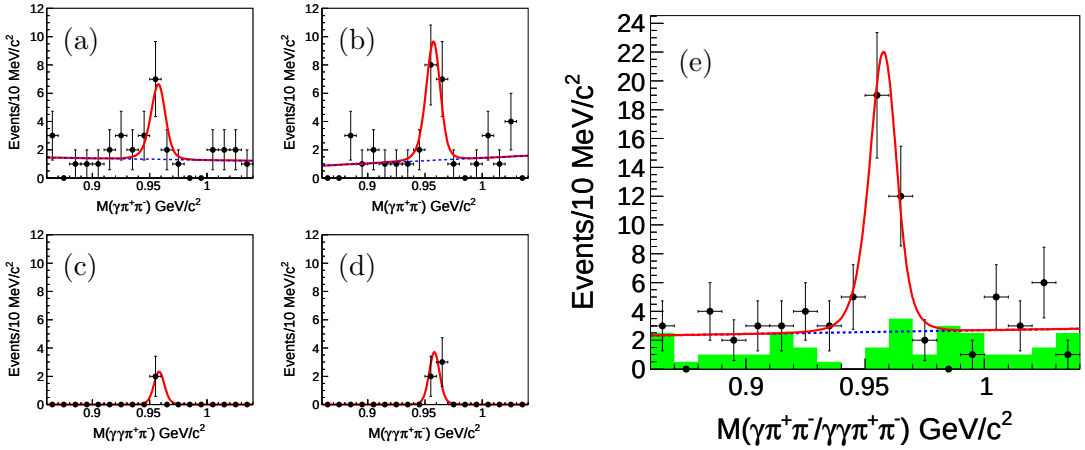

FIG. 3: Same as Fig. 2 at $\sqrt{s} = 4.260\,\text{GeV}$.

χ^2/ndf for the combined result is 0.9, where sparsely populated bins are combined so that there are at least seven counts per bin in the χ^2 calculation and ndf is the number of degrees of freedom. The fit yields $N^{\text{obs}} = 36.5 \pm 6.9$, and the statistical significance of the η' signal is determined to be 8.6σ by comparing log-likelihood values with and without η' signal in the fit and taking the change of the ndf into account. The similar fit process is performed for the data at $\sqrt{s} = 4.260\,\text{GeV}$, and corresponding results are shown in Fig 3. The χ^2/ndf for the combined result is 0.94, the fit yields $N^{\text{obs}} = 30.0 \pm 6.2$ and the statistical significance of the η' signal is 7.3σ.

The same event selection criteria is performed to the data samples taken at the other 12

energy points, $\sqrt{s} = 4.230$ and 4.260 GeV are taken out. Figure 4 depicts the scatter plot of $M(\ell^+\ell^-)$ versus $M(\gamma\pi^+\pi^-/\eta\pi^+\pi^-)$ and the projections of $M(\ell^+\ell^-)$ and $M(\gamma\pi^+\pi^-/\eta\pi^+\pi^-)$ including all 12 energy points. We can see a cluster of events in the signal region, although no significant $\eta' J/\psi$ signals are observed at individual energy point. As a consequence, the upper limits on the number of signal events at the 90% confidence level (C.L.) are set using a Bayesian method [23] at individual energy point. Here, we fit the $M(\gamma\pi^+\pi^-/\eta\pi^+\pi^-)$ with the number of signal events set from 0 to n to get a series of likelihood values. The upper limit is determined by examining the number of signal events corresponding to 90% of the likelihood distribution. The results are listed in Table I.

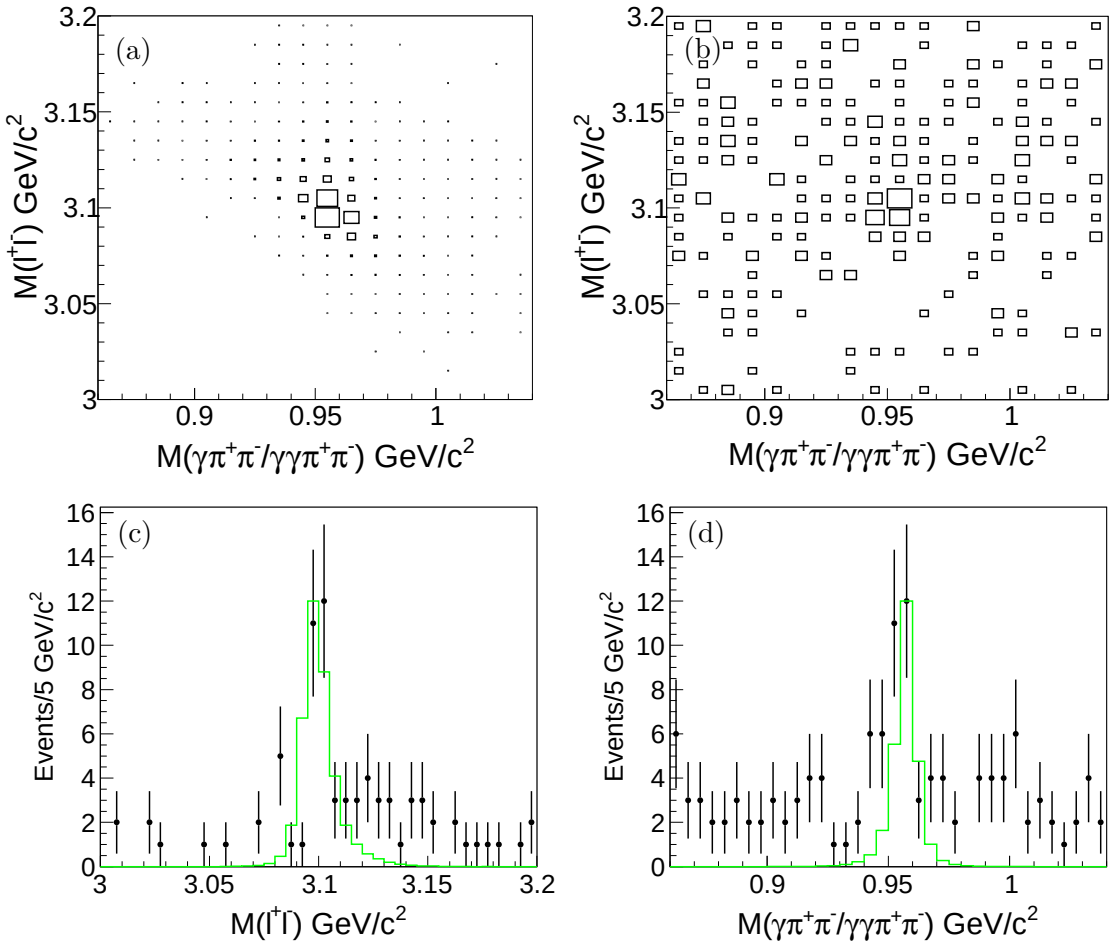

FIG. 4: The distributions for the data samples taken at $\sqrt{s} = 4.190$, 4.210, 4.220, 4.245, 4.310, 4.360, 4.390, 4.420, 4.470, 4.530, 4.575, and 4.600 GeV, (a) the scatter plot of $M(\ell^+\ell^-)$ versus $M(\gamma\pi^+\pi^-/\eta\pi^+\pi^-)$ for the MC simulation; (b) the corresponding scatter plot for the data; (c) the projection of $M(\ell^+\ell^-)$, and (d) the projection of $M(\gamma\pi^+\pi^-/\eta\pi^+\pi^-)$, in which points with error bars are data and histograms are signal MC simulation.

V. CROSS SECTION RESULTS

The Born cross section is calculated with

$$\sigma^{\rm B} = \frac{N^{\rm obs}}{L_{\rm int}\cdot(1+\delta)\cdot|1+\Pi|^2\cdot\sum_{\rm i=1}^{4}\epsilon_{\rm i}\mathcal{B}_{\rm i}}, \quad (1)$$

where $N^{\rm obs}$ is the number of observed signal events from fit, $L_{\rm int}$ is the integrated luminosity, $\epsilon_{\rm i}$ is selection efficiency for the ith channel estimated from the MC simulation, $\mathcal{B}_{\rm i}$ is the product branching fraction of intermediate states for the ith channel taken from the Particle Data Group [1], $|1+\Pi|^2$ is the vacuum polarization factor [24] and $(1+\delta)$ is the radiative correction factor, which is defined as

$$1+\delta = \frac{\int_0^1 \sigma(s(1-x))F(x,s)dx}{\sigma(s)}. \quad (2)$$

The radiative correction changes the total cross section and emission of additional photons affects the efficiency of selection. Here, x is the ratio between radiative photon's energy and the center of mass energy, $F(x,s)$ is radiator function, which is obtained from QED calculation [25] with an accuracy of 0.1% and $\sigma(s)$ is the cross section line shape of $e^+e^-\to\eta' J/\psi$, which is described by a constant width BW function with the parameters from the $\psi(4160)$ plus a polynomial function.

All the numbers used in the cross section calculation are summarized in Table I. The Born cross section is measured to be $(3.7\pm0.7\pm0.3)$ pb at 4.230 GeV and $(3.9\pm0.8\pm0.3)$ pb at 4.260 GeV, where the first errors are statistical and the second ones systematic. The Born cross sections and upper limits at other energy points are also shown in Table I. In the upper limit determination, a conservative result with a factor $1/(1-\sigma)$ is included to take into account the effect of the total systematic uncertainty, σ, which is described in the next section in detail.

Figure 5 shows the measured Born cross sections for $e^+e^-\to\eta' J/\psi$ over the energy region studied in this work. By assuming that the $\eta' J/\psi$ signals come from the $\psi(4160)$ decay, a phase space modified BW function is used to fit the data, where the parameters of the BW are fixed to the PDG values. The χ^2/ndf is 0.9, which means the measurement supports our assumption. The second resonance $\psi(4415)$ is also added in the fit, the statistical significance is determined to be 2.6σ by comparing the two $-2\ln(L)$ values and taking the change of ndf into account. It indicates that the contribution of $\psi(4415)$ is not significant.

VI. SYSTEMATIC UNCERTAINTIES

Several sources of systematic uncertainties are considered in the measurement of the Born cross section, including the integrated luminosity measurement, background shape, fitting range, ISR correction factor, photon detection, tracking efficiency, kinematic fit, lepton pair mass resolution, and the branching fractions of intermediate states decay.

(a) The uncertainty from integrated luminosity measurement using Bhabha ($e^+e^-\to e^+e^-$) events is estimated to be 1.0% [15].

TABLE I: The summary of numbers used to calculate the Born cross section of $e^+e^- \to \eta' J/\psi$. The upper limits are at the 90% C.L.

$\sqrt{s}$ (GeV)	$N^{\rm obs}$	$L_{\rm int}$ (pb^{-1})	$1+\delta$	$\sum \epsilon_{\rm i}\mathcal{B}_{\rm i}$ (10^{-2})	$\lvert 1+\Pi\rvert^2$	$\sigma^{\rm B}$ (pb)
4.190	3.8 ± 2.3 (< 8.7)	43.1	0.857	1.01	1.056	$9.7 \pm 5.8 \pm 0.6$ (< 24)
4.210	2.6 ± 3.2 (< 13.3)	54.6	0.885	1.04	1.057	$4.9 \pm 6.1 \pm 0.4$ (< 28)
4.220	1.0 ± 1.7 (< 6.2)	54.1	0.902	1.00	1.057	$1.9 \pm 3.3 \pm 0.2$ (< 14)
4.230	36.5 ± 6.9	1047.3	0.919	0.98	1.056	$3.7 \pm 0.7 \pm 0.3$
4.245	0.8 ± 1.4 (< 5.3)	55.6	0.945	0.95	1.056	$1.5 \pm 2.7 \pm 0.2$ (< 11)
4.260	30.0 ± 6.2	825.7	0.969	0.91	1.054	$3.9 \pm 0.8 \pm 0.3$
4.310	2.2 ± 1.5 (< 5.9)	44.9	1.036	0.81	1.052	$5.6 \pm 3.8 \pm 0.3$ (< 16)
4.360	3.0 ± 2.3 (< 7.9)	539.8	1.114	0.77	1.051	$0.6 \pm 0.5 \pm 0.1$ (< 1.8)
4.390	2.1 ± 2.1 (< 8.3)	55.2	1.162	0.73	1.051	$4.3 \pm 4.3 \pm 0.3$ (< 18)
4.420	10.8 ± 4.1(< 15.9)	1028.9	1.191	0.71	1.053	$1.2 \pm 0.5 \pm 0.1$ (< 1.9)
4.470	5.9 ± 4.1 (< 14.8)	109.9	1.161	0.72	1.055	$6.1 \pm 4.2 \pm 0.5$(< 17)
4.530	1.4 ± 1.3 (< 5.3)	110.0	1.002	0.81	1.055	$1.5 \pm 1.4 \pm 0.1$ (< 6.0)
4.575	0.0 ± 1.7 (< 9.0)	47.7	0.907	0.90	1.055	$0.0 \pm 4.2 \pm 0.4$(< 24)
4.600	1.2 ± 2.3 (< 7.9)	566.9	0.880	0.92	1.055	$0.3 \pm 0.5 \pm 0.1$ (< 1.8)

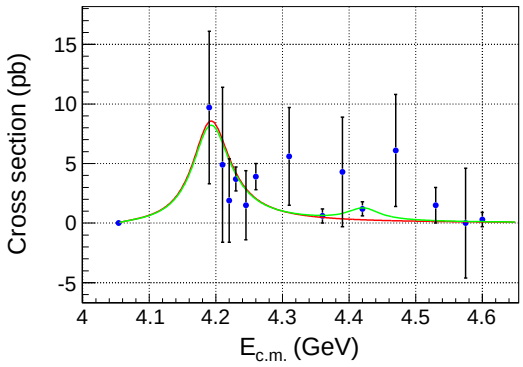

FIG. 5: Fit to the Born cross section $\sigma(e^+e^- \to \eta' J/\psi)$ with a $\psi(4160)$ resonance (red curve), or a combination of $\psi(4160)$ and $\psi(4415)$ resonances (green curve). The uncertainties are statistical only.

(b) The systematic uncertainty due to the background shape is estimated by varying the background shape from a linear function to a second order Chebyshev polynomial. The difference in the signal yields is taken as the systematic uncertainty.

(c) The systematic uncertainty from the fitting range is estimated by varying the fitting range from $[0.86, 1.04]$ GeV to $[0.87, 1.05]$ GeV or $[0.85, 1.03]$ GeV. The largest change in the signal yields is taken as the systematic uncertainty.

Since the relative signal yield for individual decay mode is constrained by the factor of $\epsilon_{\rm i}\mathcal{B}_{\rm i}$ in the fit procedure, the uncertainties due to $\epsilon_{\rm i}$ or $\mathcal{B}_{\rm i}$ affect not only $\epsilon_{\rm i}\mathcal{B}_{\rm i}$ but also $N^{\rm obs}$. Taking both terms into account, we change the values of $\epsilon_{\rm i}$ or $\mathcal{B}_{\rm i}$, then refit the data. The change of the measured cross section is taken as the systematic uncertainty.

(d) The ISR correction factors are obtained by QED calculation and the cross section measured by this analysis, which is parameterized by a BW function of $\psi(4160)$ plus a polynomial function. The ISR correction factors are calculated iteratively until they become stable. To estimate the uncertainty due to the ISR correction factor, the measured cross section is also parameterized by a BW function or a polynomial function. The largest discrepancy between the alternative assumptions and the nominal result is taken as the systematic error.

(e) The uncertainty due to photon reconstruction efficiency is 1.0% per photon [26]. Therefore, we vary the values of $\epsilon_{\rm i}$ up or down by $1\% \times N_\gamma$ and refit the data, where N_γ is the number of photons in final states. The maximum change of the measured cross section is taken as the systematic uncertainty.

(f) The discrepancy of tracking efficiency between the MC simulation and the data is estimated to be 1.0% per charged track from a study of $e^+e^- \to \pi^+\pi^- J/\psi$ and $e^+e^- \to 2(\pi^+\pi^-)$. There are 4 charged tracks in the candidate events, 4.0% is adopted as the changed value for $\epsilon_{\rm i}$. Actually, the four decay channels have a similar uncertainty on the tracking efficiency and are 100% correlated, so the total change in the final results is 4%.

(g) The mass resolution discrepancy between the MC simulation and the data will introduce uncertainty when we apply a mass window requirement on the invariant mass distribution of lepton pairs. This uncertainty is estimated using the control sample $e^+e^- \to \gamma_{\rm ISR}\psi(3686) \to \gamma_{\rm ISR}\pi^+\pi^- J/\psi$ with $J/\psi \to e^+e^-$ or $\mu^+\mu^-$. The same J/ψ mass window $[3.07, 3.13]\,{\rm GeV}$ is required for both the data and the MC sample, the difference of efficiency is adopted in the uncertainty estimation.

(h) The uncertainty associated with the kinematic fit arises from the inconsistency of track helix parameters between the data and the MC simulation. Therefore, three track parameters, ϕ_0, κ and $\tan\lambda$ are corrected in the signal MC simulation. The correction factors are obtained by comparing their pull distributions in the control sample and the MC simulation [27]. The difference of the detection efficiency between the samples with and without the helix correction is regarded as the systematic uncertainty.

(i) The branching fractions of $J/\psi \to e^+e^-/\mu^+\mu^-$, $\eta' \to \gamma\pi^+\pi^-/\eta\pi^+\pi^-$, and $\eta \to \gamma\gamma$ are changed independently, then fit the data set. The quadrature sum of all uncertainties due to the branching fractions is taken as the systematic uncertainty.

(j) The final state radiation effect only affects the lepton pair invariant mass distribution and the kinematic fit efficiency, its systematic uncertainty is included already. Other sources such as the E/p ratio requirement for electron and muon separation and c.m. energy measurement are estimated to be less than 1% and are neglected in this analysis.

The sources of systematic uncertainty and their contributions are summarized in Table II. The total systematic uncertainty is the quadrature sum of all individual uncertainties.

VII. SUMMARY

In summary, the process $e^+e^- \to \eta' J/\psi$ is investigated using data samples collected with the BESIII detector at 14 c.m. energies from 4.19 to 4.60 GeV. Significant $e^+e^- \to \eta' J/\psi$ signals are observed at $\sqrt{s} = 4.230$ and 4.260 GeV, and the corresponding Born cross sections are measured to be $(3.7 \pm 0.7 \pm 0.3)$ and $(3.9 \pm 0.8 \pm 0.3)$ pb, respectively. The upper limits

TABLE II: Summary of systematic uncertainties (%).

Source/$\sqrt{s}$ (GeV)	4.190	4.210	4.220	4.230	4.245	4.260	4.310	4.360	4.390	4.420	4.470	4.530	4.575	4.600
Luminosity measurement	1.0	1.0	1.0	1.0	1.0	1.0	1.0	1.0	1.0	1.0	1.0	1.0	1.0	1.0
Background shape	0.1	3.4	5.3	0.2	4.9	2.4	0.1	0.2	0.6	4.6	0.1	0.2	0.0	2.9
Fitting range	0.4	4.1	2.7	2.2	0.7	2.2	0.3	5.1	0.2	7.7	6.1	1.2	0.0	3.5
ISR factor	3.0	1.2	3.0	4.0	4.4	1.1	2.5	2.1	2.9	1.7	1.5	2.9	6.0	2.1
Photon detection	1.1	1.1	1.1	1.4	1.1	1.3	1.2	1.2	1.1	1.4	1.5	1.1	1.1	1.1
Tracking efficiency	4.0	4.0	4.0	4.0	4.0	4.0	4.0	4.0	4.0	4.0	4.0	4.0	4.0	4.0
Kinematic fitting	1.1	1.6	1.4	1.1	1.2	1.0	1.1	0.6	1.3	0.8	1.9	1.4	0.5	1.7
Lepton pair mass resolution	2.0	3.7	1.1	2.2	2.6	2.0	1.7	2.6	1.1	1.7	2.6	2.4	3.6	1.3
Branching fraction	1.9	1.9	1.9	1.6	2.0	1.5	1.7	1.6	1.9	1.5	1.6	3.4	1.8	1.8
Total	6.1	8.3	8.4	7.0	8.7	6.2	5.7	7.7	5.8	10.4	8.5	6.9	8.4	7.1

of Born cross sections at the 90% C.L. are set for the other 12 c.m. energy points where no significant signal is observed. The measured cross sections support the signals of $\eta' J/\psi$ come from $\psi(4160)$ decays, and the contribution of $\psi(4415)$ is not evident.

Comparing with the measurement of $e^+e^- \to \eta J/\psi$ [10], the Born cross section of $e^+e^- \to \eta' J/\psi$ is much smaller, which is in contradiction to the calculation in Ref. [12]. There are two possible reasons contributing to the discrepancy. The cross section of $e^+e^- \to \eta' J/\psi$ is investigated at order of $O(\alpha_s^4)$, therefore, higher order correction might need to be considered; gluonium component contributions may affect the results significantly, requiring the proportion of gluonic admixture in η' to be further studied.

Acknowledgments

The BESIII collaboration thanks the staff of BEPCII and the IHEP computing center for their strong support. This work is supported in part by National Key Basic Research Program of China under Contract No. 2015CB856700; National Natural Science Foundation of China (NSFC) under Contracts Nos. 11125525, 11235011, 11322544, 11335008, 11425524; the Chinese Academy of Sciences (CAS) Large-Scale Scientific Facility Program; Joint Large-Scale Scientific Facility Funds of the NSFC and CAS under Contracts Nos. 11179007, U1232201, U1332201; CAS under Contracts Nos. KJCX2-YW-N29, KJCX2-YW-N45; 100 Talents Program of CAS; INPAC and Shanghai Key Laboratory for Particle Physics and Cosmology; German Research Foundation DFG under Contract No. Collaborative Research Center CRC-1044; Istituto Nazionale di Fisica Nucleare, Italy; Ministry of Development of Turkey under Contract No. DPT2006K-120470; Russian Foundation for Basic Research under Contract No. 14-07-91152; U. S. Department of Energy under Contracts Nos. DE-FG02-04ER41291, DE-FG02-05ER41374, DE-FG02-94ER40823, DE-SC0010118; U.S. National Science Foundation; University of Groningen (RuG) and the Helmholtzzentrum fuer Schwerionenforschung GmbH (GSI), Darmstadt; WCU Program of National Research Foundation of Korea under Contract No. R32-2008-000-10155-0.

[1] K. A. Olive *et al.* [Particle Data Group], Chin. Phys. C **38**, 090001 (2014).

[2] B. Aubert *et al.* [BABAR Collaboration], Phys. Rev. Lett. **95**, 142001 (2005); J. P. Lees *et al.* [BABAR Collaboration], Phys. Rev. D **86**, 051102(R) (2012).

[3] B. Aubert *et al.* [BABAR Collaboration], Phys. Rev. Lett. **98**, 212001 (2007); J. P. Lees *et al.* [BABAR Collaboration], Phys. Rev. D **89**, 111103(R) (2014).

[4] C. Z. Yuan *et al.* [Belle Collaboration], Phys. Rev. Lett. **99**, 182004 (2007); Z. Q. Liu *et al.* [Belle Collaboration], Phys. Rev. Lett. **110**, 252002 (2013).

[5] X. L. Wang *et al.* [Belle Collaboration], Phys. Rev. Lett. **99**, 142002 (2007); G. Pakhlova *et al.* [Belle Collaboration], Phys. Rev. Lett. **111**, 172001 (2008); X. L. Wang *et al.* [Belle Collaboration], Phys. Rev. D **91**, no. 11, 112007 (2015).

[6] Q. He *et al.* [CLEO Collaboration], Phys. Rev. D **74**, 091104(R) (2006).

[7] For a recent review, see N. Brambilla *et al.*, Eur. Phys. J. C **71**, 1534 (2011).

[8] T. E. Coan *et al.* [CLEO Collaboration], Phys. Rev. Lett. **96**, 162003 (2006).

[9] X. L. Wang *et al.* [Belle Collaboration], Phys. Rev. D **87**, 051101 (2013).

[10] M. Ablikim *et al.* [BESIII Collaboration], Phys. Rev. D **86**, 071101 (2012); M. Ablikim *et al.* [BESIII Collaboration], Phys. Rev. D **91**, 112005 (2015).

[11] Q. Wang, X. -H. Liu and Q. Zhao, Phys. Rev. D **84**, 014007 (2011).

[12] C. F. Qiao, R. L. Zhu, Phys. Rev. D **89**, 074006 (2014).

[13] M. Ablikim *et al.* [BESIII Collaboration], arXiv:1510.08654 [hep-ex], submitted to Nucl. Instrum. Meth. A.

[14] M. Ablikim *et al.* [BESIII Collaboration], Nucl. Instrum. Meth. A **614**, 345 (2010).

[15] M. Ablikim *et al.* [BESIII Collaboration], arXiv:1503.03408.

[16] J. Z. Bai *et al.* [BES Collaboration], Nucl. Instrum. Meth. A **458**, 627 (2001); **344**, 319 (1994).

[17] D. M. Asner *et al.*, Int. J. Mod. Phys. A **24**, S1 (2009).

[18] S. Agostinelli *et al.* [GEANT4 Collaboration], Nucl. Instrum. Meth. A **506**, 250 (2003).

[19] S. Jadach, B. F. L. Ward and Z. Was, Phys. Rev. D **63**, 113009 (2001).

[20] R. G. Ping, Chin. Phys. C **32**, 599 (2008).

[21] J. C. Chen, G. S. Huang, X. R. Qi, D. H. Zhang and Y. S. Zhu, Phys. Rev. D **62**, 034003 (2000).

[22] http://home.thep.lu.se/∼torbjorn/Pythia.html

[23] J. Conrad *et al.*, Phys. Rev. D **67**, 012002 (2003).

[24] S. Actis *et al.* [Working Group on Radiative Corrections and Monte Carlo Generators for Low Energies Collaboration], Eur. Phys. J. C **66**, 585 (2010).

[25] E. A. Kuraev and V. S. Fadin, Sov. J. Nucl. Phys. **41**, 466 (1985) [Yad. Fiz. **41**, 733 (1985)].

[26] M. Ablikim *et al.* [BESIII Collaboration], Phys. Rev. D **81**, 052005 (2010).

[27] M. Ablikim *et al.* [BESIII Collaboration], Phys. Rev. D **87**, 012002 (2013).